Rapid Communications

Atomic-scale mechanism of internal structural relaxation screening at polar interfaces

Mingqiang Li,[1,2] Xiaoxing Cheng,[3] Ning Li,[1,2] Heng-Jui Liu,[4] Yen-Lin Huang,[5] Kaihui Liu,[2,6,7] Ying-Hao Chu,[5,8] Dapeng Yu,[6,7,9] Long-Qing Chen,[3] Yuichi Ikuhara,[10,11] and Peng Gao[1,2,6,*]

[1]*Electron Microscopy Laboratory, and International Center for Quantum Materials, School of Physics, Peking University, Beijing 100871, China*

[2]*Academy for Advanced Interdisciplinary Studies, Peking University, Beijing 100871, China*

[3]*Department of Materials Science and Engineering, The Pennsylvania State University, University Park, Pennsylvania 16802, USA*

[4]*Department of Materials Science and Engineering, National Chung Hsing University, Taichung 40227, Taiwan, Republic of China*

[5]*Department of Materials Science and Engineering, National Chiao Tung University, Hsinchu 30010, Taiwan, Republic of China*

[6]*Collaborative Innovation Centre of Quantum Matter, Beijing 100871, China*

[7]*State Key Laboratory for Mesoscopic Physics, School of Physics, Peking University, Beijing 100871, China*

[8]*Institute of Physics, Academia Sinica, Taipei 11529, Taiwan, Republic of China*

[9]*Department of Physics, South University of Science and Technology of China, Shenzhen 518055, China*

[10]*Institute of Engineering Innovation, The University of Tokyo, Tokyo 113-8656, Japan*

[11]*Nanostructures Research Laboratory, Japan Fine Ceramic Centre, Nagoya 456-8587, Japan*

(Received 5 September 2017; revised manuscript received 28 April 2018; published 25 May 2018)

The effective screening of the polarization bound charge is a prerequisite to stabilize the ferroelectricity in ferroelectric thin films. Here, by combining annular bright field imaging and electron energy-loss spectroscopy (EELS) in an aberration-corrected scanning transmission electron microscope with phase-field simulations, we investigate the screening mechanism by quantitatively measuring the structural relaxation at $Pb(Zr_{0.2}Ti_{0.8})O_3/SrTiO_3$ interfaces. We find that the thickness of the interfacial layer is ~3.5 unit cells (~1.4 nm) in a domain with upward polarization and ~5.5 unit cells (~2.2 nm) in a domain with downward polarization. Phase-field simulations, an EELS analysis, and a lattice parameter analysis verify the existence of interfacial oxygen vacancies accounting for the narrower interfacial layer in the domain with upward polarization. Our study indicates the internal structural relaxation at the interface is the dominant mechanism for the polarization charge screening for ferroelectric films grown on insulating substrates and has implications for our understanding of domain switching in ferroelectric devices.

DOI: 10.1103/PhysRevB.97.180103

At the physical boundaries of ferroelectrics (e.g., the surface and heterointerface), the discontinuities of dipole moments cause a bound charge, leading to a depolarization field that is opposite to the polarization orientation and which destabilizes the ferroelectric phase [1,2]. To retain stable polarization [3], the bound charge at the ferroelectric boundaries must be compensated by a redistribution of free carriers, structural distortion, electronic reconstruction, or the formation of domain stripes to reduce the energy of the depolarization field [4,5]. Therefore, the nature of ferroelectric boundaries is largely governed by screening mechanisms. For bulk ferroelectrics, the contribution of ferroelectric boundaries to the macroscopic properties is minor and therefore the screening details are usually disregarded [6,7]. However, for nanoscale devices (e.g., thin films) in which the free energies of boundary screening are comparable to that of the bulk and thus the properties of boundaries may dominate the response of the entire device. The screening mechanisms and properties of ferroelectric boundaries become vital. For example, in thin films, surface screening via absorption can induce polarization switching [8]. The screening at a ferroelectric-electrode interface usually favors one polarization orientation and suppresses the other one, leading to spontaneous retention loss [9,10]. For ultrathin ferroelectric films, there exists a critical thickness below which ferroelectricity disappears due to incomplete screening at the surface and/or interface [2,11]. Furthermore, ferroelectric domain switching must be accompanied with a charge redistribution to screen the polarization bound charge [12,13].

The screening mechanisms can be categorized as (1) external screening from outside the physical ferroelectric boundary and (2) internal screening from the ferroelectric itself [5]. For both, polarization charge compensation can be in the form of a charge redistribution or structural relaxation (or typically both). For example, for $PbTiO_3$ thin films on ideal conducting $SrRuO_3$ (SRO) or a Pt substrate, electrons from the metallic substrate can act as an external screening charge [14], and, meanwhile, ferroelectric polarization changes abruptly at the interface and no structural relaxation is needed in either the ferroelectrics or substrate/electrode. However, in most practical devices (thin films), external screening is not ideal and a structural relaxation at the interface of ferroelectric heterostructures is also required [15], which may play an important role in determining domain nucleation [16,17] and domain stability [18,19].

*p-gao@pku.edu.cn

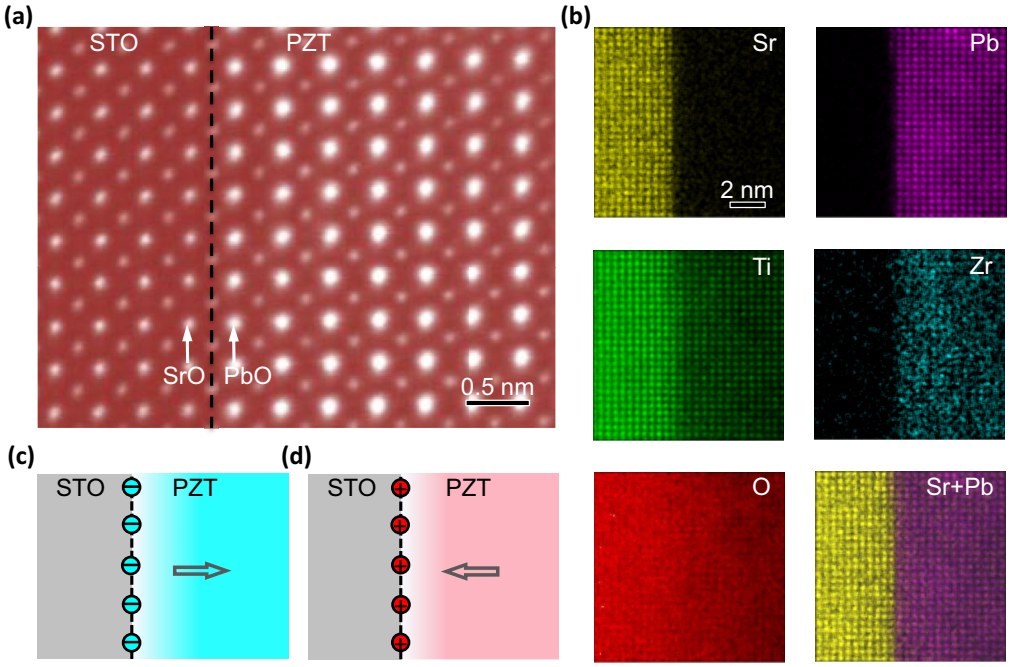

FIG. 1. Atomic structure of a $Pb(Zr_{0.2}Ti_{0.8})O_3/SrTiO_3$ (PZT/STO) interface. (a) An atomically resolved high-angle annular dark field (HAADF) image of a PZT film on a STO substrate. The viewing direction is along [010]. The dashed line shows the position of the interface, TiO_2 plane, between the first SrO and PbO planes. (b) Atomically resolved energy dispersive x-ray spectroscopy (EDS) maps for Sr, Pb, Ti, Zr, and O of the PZT/STO interface. No distinguishable interdiffusion of cations Pb and Sr is observed. (c) Schematic shows the negative polarization bound charge at the interface with upward polarization (refers to the substrate). (d) Schematic shows the positive polarization bound charge at the interface with downward polarization (refers to the substrate).

Revealing the details of internal screening is usually difficult because the strong spatial variety in multidomain structures makes those bulk-based techniques such as x-ray or electrical characterization no longer suitable to study polarization-dependent interfacial structures [20]. On the other hand, commonly used surface techniques such as scanning tunneling microscopy (STM) or piezoelectric force microscopy (PFM) are unable to detect the properties of the buried interface [21,22]. In contrast, recent advancements in aberration-corrected scanning transmission electron microscopy (STEM) have made it possible to directly reveal the interface structures [23–33], e.g., the unit-cell scaled interfacial "dead layer" [30,34–36]. In fact, these reported thicknesses of dead layers are not consistent even for the same sample system [30,34,35], probably due to a strong dependence on microstructures.

In this Rapid Communication, we focus on $Pb(Zr_{0.2}Ti_{0.8})O_3$ (PZT) films grown on (001) $SrTiO_3$ (STO) insulating substrates and demonstrate polarization orientation-dependent structural relaxation at the polar interfaces. By using atomically resolved annular bright field (ABF) imaging in aberration-corrected STEM with sub-50 pm resolutions, the positions of both O and heavy cations can be determined, enabling precise measurements of the structural parameters at the buried interface [23]. We find that since the STO substrate cannot provide enough external charge for screening, the polarization bound charge at the interface is partially compensated by an internal structural relaxation to form transition layers with a suppression of polarization at the interface. At the interface in the upward domain (with polarization pointing to a free surface), the internal screening layer is about 3.5 unit cells (∼1.4 nm), while the thickness of the relaxed layer is about 5.5 unit cells (∼2.2 nm) at the interface in the downward domain (with polarization pointing to the substrate). The phase-field simulation indicates that the distribution of oxygen vacancies accounts for this polarization orientation-dependent structural relaxation in ferroelectric/insulator systems, which is further evidenced by EELS and a lattice parameter analysis. The results suggest the structural relaxation that commonly exists at the ferroelectric boundaries is polarization orientation-dependent, which helps to explain many ferroelectric phenomena such as interface-assisted domain nucleation [16,17] and interface-induced domain retention loss [19] in ferroelectric thin films.

A high-angle annular dark field (HAADF) image of PZT films on a (001) STO substrate is shown in Fig. 1(a), from which only the cations (Pb and ZrO/TiO) are visible. In the *Z*-contrast HAADF image, we can easily determine the location of the interface, TiO_2 plane, between the first SrO and PbO planes. The atomically resolved energy dispersive x-ray spectroscopy (EDS) maps for Sr, Pb, Ti, Zr, and O indicate the PZT/STO interface is atomically sharp, i.e., the interdiffusion between Sr and Pb is less than one unit cell in Fig. 1(b). For PZT, the polarization arises from the displacements between the cations and anion O. At the interface, the accumulation of negative and positive polarization bound charge by intrinsic ionic displacements is shown vividly in Figs. 1(c) and 1(d), respectively, i.e., negative bound charge at the bottom interface with upward ferroelectric polarization while positive bound charge for downward ferroelectric polarization.

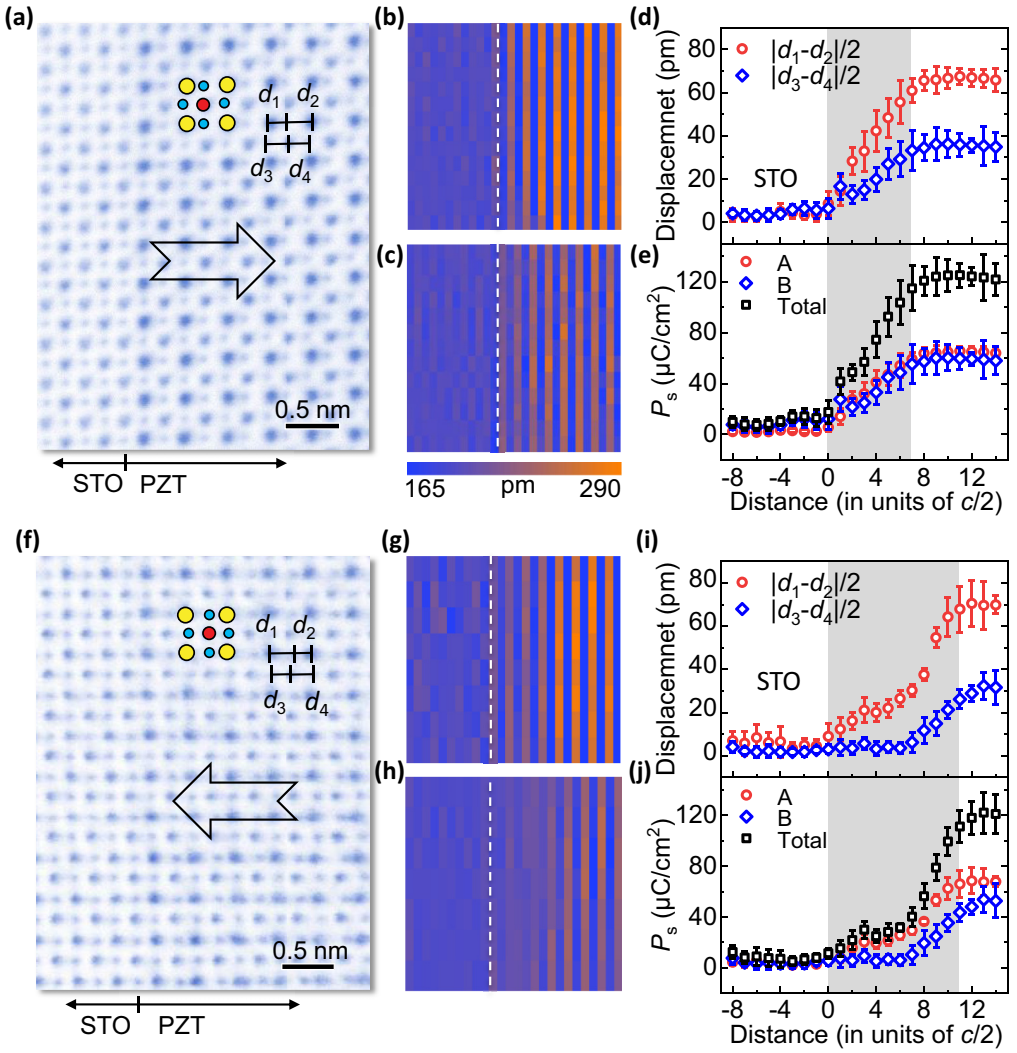

FIG. 2. Quantitative measurements of structural relaxation at PZT/STO interfaces. (a) An annular bright field (ABF) image of a PZT thin film with upward polarization, which is indicated by an open arrow. The schematic is overlaid with the ABF image. Red disk: Ti/ZrO column. Yellow disk: Pb column. Blue disk: O column. The calculated bond lengths d_1 and d_2 (b) in the AO plane and d_3 and d_4 (c) in the BO_2 plane. A: Sr, Pb. B: Ti/Zr. (d) Mean of displacements of $|d_1 - d_2|/2$ and $|d_3 - d_4|/2$. The error bar is the standard deviation (s.d.). (e) Averaged polarization calculated from the displacements in a PbO plane, TiO_2 plane, and the total. The transition zone is indicated by the gray color. The error bar is the s.d. (f) An ABF image of a PZT thin film with downward polarization, which is indicated by an open arrow. The schematic is overlaid with the ABF image. Red disk: Ti/ZrO column. Yellow disk: Pb column. Blue disk: O column. The calculated bond lengths d_1 and d_2 (g) in the AO plane and d_3 and d_4 (h) in the BO_2 plane. (i) Mean of displacements of $|d_1 - d_2|/2$ and $|d_3 - d_4|/2$. The error bar is the s.d. (j) Averaged polarization calculated from the displacements in a PbO plane, TiO_2 plane, and the total. The transition zone is indicated by the gray color. The error bar is the s.d.

The ABF image in Fig. 2(a) shows an interface in the upward domain. The bond lengths of Pb-O and Ti-O are marked with d_1,d_2,d_3, and d_4 in Fig. 2(a). A schematic of tetragonal PZT and a definition of d_1,d_2,d_3 and d_4 are provided in Fig. S1 [37]. The spontaneous polarization in each unit cell can be calculated precisely from

$$\delta p = \frac{e}{\Omega}\sum_{m=1}^{N} z_m \delta u_m, \tag{1}$$

where e is the elementary charge, N is the number of atoms in the primitive unit cell, Ω is the volume of the unit cell, Z_m is the Born effective charge [38], and δu_m is the first-order change of the position vector of the mth basis atom which can be calculated from d_1,d_2,d_3, and d_4. The Pb-O bond lengths d_1 and d_2 are shown in Fig. 2(b) and the Ti-O bond lengths d_3 and d_4 are shown in Fig. 2(c), respectively. Both maps appear with periodic stripes in the PZT films due to the alternate long and short bond lengths between the cations and the anion. The plotted atomic displacements between the cations and the anion in Fig. 2(d) gradually increase from zero at the interface to the level of the bulk PZT film. Note that the displacement of Pb with respect to O is much larger than that of Ti with respect to O [23]. Based on the reported values of the Born effective charges [38], the polarization of the PbO and TiO_2 planes, and total polarization are calculated in Fig. 2(e). The transition

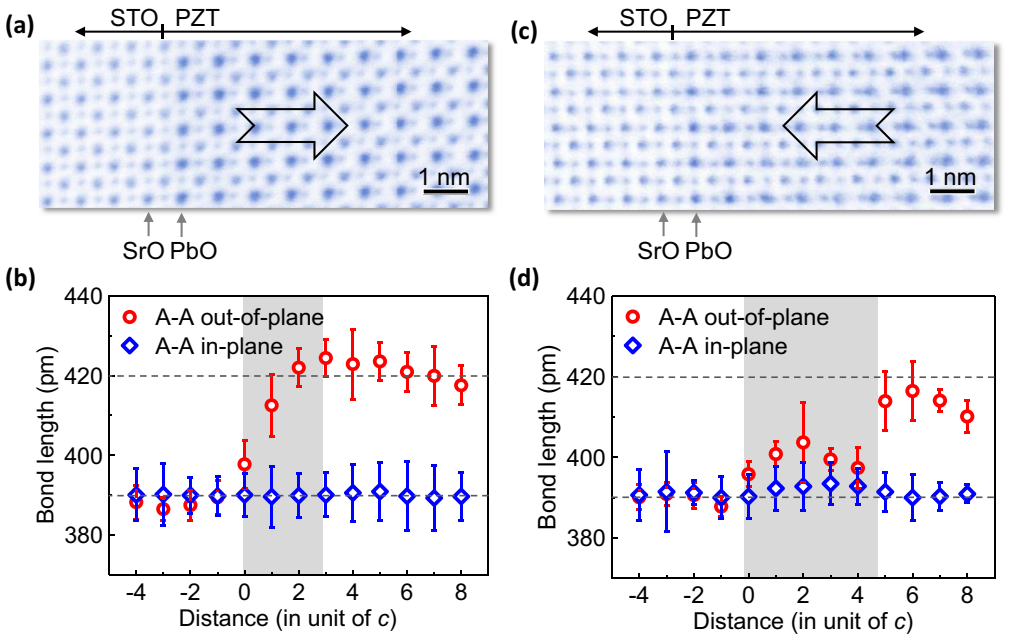

FIG. 3. Lattice parameters measured from ABF images. (a) An ABF image of the upward domain in a PZT thin film. (b) Profiles of out-of-plane (red circle) and in-plane (blue diamond) lattices obtained from the image in (a), averaged over vertical atomic rows of the image. The interfacial structure relaxation layer is indicated by the gray color. The error bar is the s.d. (c) An ABF image of the downward domain in a PZT thin film. (d) Profiles of out-of-plane (red circle) and in-plane (blue diamond) lattices obtained from the image in (c), averaged over vertical atomic rows of the images. The interfacial structure relaxation layer is indicated by the gray color. The error bar is the s.d.

area with suppressed polarization is about 3.5 unit cells in thickness.

Although the polarization in the as-grown PZT film is mainly upward, one small domain with downward polarization is also observed in Fig. 2(f) (more than 190 STEM images along the interface are analyzed and only two images show downward polarization). We did a similar analysis of this image to further explore the relationship between structural relaxation and polarization orientation in PZT films. The Pb-O and Ti-O bond length maps are shown in Figs. 2(g) and 2(h), respectively. The mean of displacements plotted in Fig. 2(i) shows the width of structural relaxation is about 5.5 unit cells in the downward domain. Moreover, the displacement of Ti is very small in the first three unit cells, meaning the polarization in the TiO_2 plane is even more significantly suppressed. The polarization in PZT is usually associated with tetragonality [39,40]. We therefore measure the lattice parameter at the PZT/STO interfaces for both of the upward [Figs. 3(a) and 3(b)] and downward [Figs. 3(c) and 3(d)] domains. The PZT has a larger out-of-plane lattice parameter compared to the STO, while the in-plane lattice parameter remains the same owing to epitaxial growth. Although tetragonality at the interfaces of both of domains is suppressed, the width of the interfacial area with reduced tetragonality is different between the upward and downward domains, i.e., it is about 3.5 unit cells in the upward domain and about 5.5 unit cells in the downward domain, being consistent with the polarization distribution at the interfaces.

Usually, for ferroelectric thin films on insulating substrates such as PZT on STO, the formation of stripe domains or atomic displacements in the substrate are required to retain the ferroelectric phase [41]. However, neither 180° stripe domains nor a structural relaxation in the substrate are observed in our PZT/STO heterostructure. In fact, the monodomainlike structure in PZT/STO was also reported in previous studies of electron microscopy [29] and x-ray diffraction [14] in which the presence of interfacial oxygen vacancies was proposed to be the mechanism [29]. The oxygen vacancies that have a positive charge likely favor upward polarization. Phase-field modeling was carried out to simulate such scenarios of interfacial oxygen vacancies at the PZT/STO heterointerfaces, as shown in Fig. 4. The Nernst-Plank equation and time-dependent Ginzburg-Landau (TDGL) equation are solved iteratively [42,43], from which we get the oxygen vacancy and polarization distribution at the same time. In order to compensate the negative bound charge at the interface with upward polarization, oxygen vacancies are pulled to the region and they reached a maximum value of about $2 \times 10^{21}/\mathrm{cm}^3$, two orders of magnitude larger than the initial concentration of $5 \times 10^{19}/\mathrm{cm}^3$. For the downward polarization case, oxygen vacancies are pushed away from the interface with a minimum value at the interface of almost 0 (details of the phase-field simulations are described in the Supplemental Material [37]).

To verify the presence of interfacial oxygen vacancies, we also perform EELS experiments for PZT/STO interfaces in the upward domain. A high-angle annular dark field (HAADF) image shows the area for EELS (see Supplemental Material [37]). The EELS experiments were carried out in a cold field gun JEM ARM200CF (JEOL Ltd.) equipped with a dual Enfinium camera (Gatan). All the spectra were recorded at 200 kV. The acquisition time is 0.1 s/pixel and the energy dispersion is 0.1 eV. The convergence semiangle is 24 mrad, and the collection angle is 53 mrad. We obtained a Ti $L_{2,3}$ edge

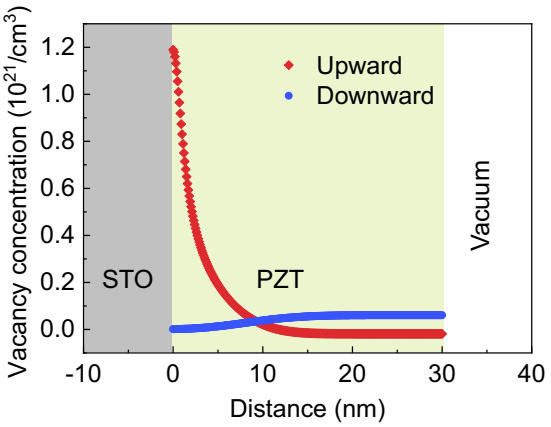

FIG. 4. Phase-field simulation result. Oxygen vacancy concentration (per cm^3) for upward and downward polarization cases in a PZT/STO heterostructure is plotted respectively as a function of distance from the interface. The red diamond indicates the oxygen vacancy concentration of the domain with upward polarization, while the blue circle indicates the oxygen vacancy concentration of the domain with downward polarization. The oxygen vacancy is stable for the upward polarization case, while it is disfavored for the downward polarization case.

and O K edge as shown in Fig. 5(a). Compared to the Ti $L_{2,3}$ edge in PZT film in Fig. 5(b), the peak splitting of the Ti L_3 and L_2 edges at the interface becomes less pronounced, which is attributed to the presence of Ti^{3+} and therefore suggests the presence of oxygen vacancies at the interface. The flatter peaks in the O K edge at the interface are also indicative of oxygen vacancies [44–46]. Furthermore, the calculated intensity of the O K edge for the PZT/STO heterostructure in Fig. 5(c) shows a valley at the interface, which further proves the presence of oxygen vacancies at the interface. Indeed, the existence of an interfacial oxygen vacancy in the upward domain is also consistent with the measurement of the lattice parameter in Fig. 3. We note that the out-of-plane lattice parameter at the interfacial layer in the upward domain is larger than that in the downward domain while the in-plane lattice remains ~390 pm in two domains due to epitaxial constraints from the STO substrate, as shown in Fig. 3. Since the lattice parameter at the interface of these perovskite heterostructures is manipulated by oxygen vacancies due mainly to the Vegard effect [31,47,48], less suppressed interfacial tetragonality of the upward domain suggests the presence of oxygen vacancies.

Therefore, the asymmetric thickness of the interfacial layers between the upward and downward domains can be understood by the charge density at the interface. For an interface with downward polarization, the total charge is P, which is a pure polarization bound charge because the oxygen vacancies are pushed away and the free carriers can be negligible in the insulating system. Meanwhile, at the interface of an upward domain with interfacial oxygen vacancies (corresponding to

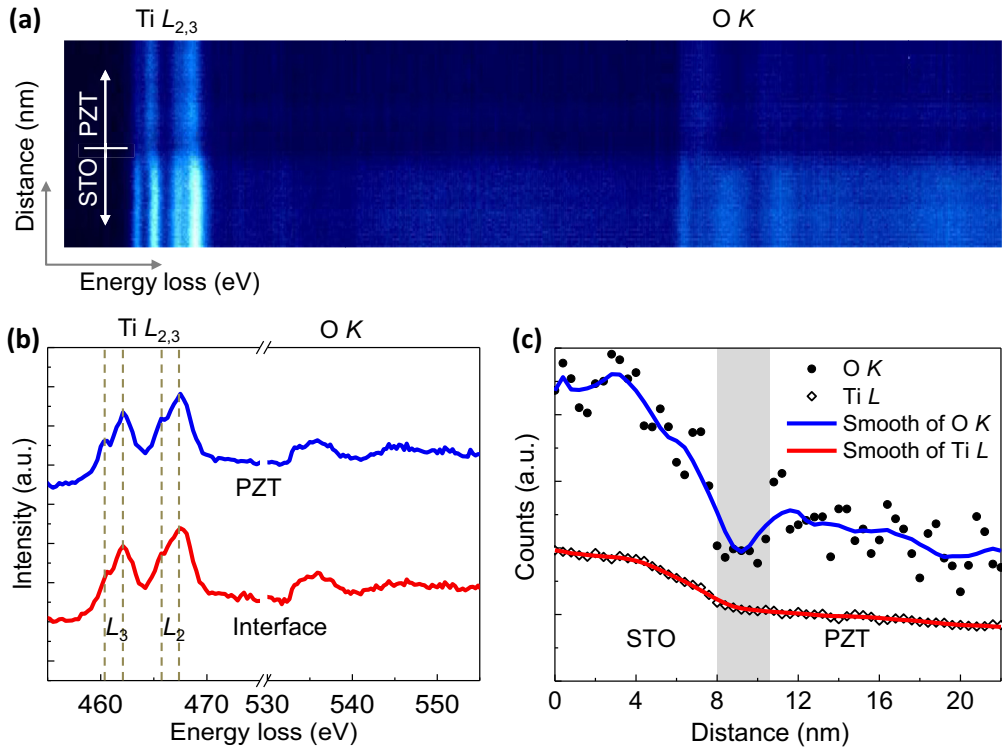

FIG. 5. Electron energy loss spectra (EELS) of a PZT/STO heterostructure. (a) EELS line scan of the Ti $L_{2,3}$ and O K edges from the interface with upward polarization. (b) Ti $L_{2,3}$ and O K edges acquired from the interfacial layer and PZT film. The blue (top) spectrum is obtained from a PZT film while the red (bottom) spectrum is obtained from the interface. The splitting of the Ti L edge becomes less pronounced at the interface, which is indicative of oxygen vacancies at the interface. (c) The areal density of Ti $L_{2,3}$ and O K edges for a PZT/STO interface. The solid circle indicates the intensity of the O K edge. The open diamond indicates the intensity of the Ti $L_{2,3}$ edge. The red line and blue line correspond to the smoothed intensity of the Ti $L_{2,3}$ and O K edges, respectively. The gray region roughly highlights the interfacial structural relaxation layer.

the charge Q), the total charge is P–Q, which is smaller than that at the interface of the downward domain. For the larger amount of charge at the interface with downward polarization, the formation of a relatively wider transition zone with a relaxed structure is likely favorable in order to reduce the charge density at the interface to further minimize the total energy. Therefore, a thicker interfacial layer with a suppression of polarization is observed at the interface of the downward domain, which is similar to the previously observed thicker transition zone at the charged domain wall [13]. Conversely, a thinner interfacial transition layer is expected if more charge can be provided at the interface to compensate the polarization charge either from the substrate or the ferroelectric itself. In fact, for the PZT film on a STO substrate with an SRO bottom electrode [49], the interfacial transition layer becomes as thin as 1.5 unit cells, even if the polarization is downward because the conducting SRO can provide many charges to screen the polarization, and thus the internal structural relaxation is no longer the dominant component for compensation (see Supplemental Material [37]).

Such polarity and charge of the interface (random field) can cause an asymmetric barrier for domain switching and affect the shape and voltage offset of the hysteresis loop, which was directly observed by previous *in situ* TEM experiments [16,17]. During ferroelectric domain switching, besides domain nucleation, the domain shape and domain wall energy (charged or uncharged) are also likely affected by the polarity and charge at the interface [17,19]. Furthermore, such an asymmetric interface nature always favors one polarization direction and destabilizes the other one, causing domain retention loss [10,19]. In fact, these deleterious effects are the main challenges for the implementation of ferroelectric devices [50].

In summary, we determine the atomic details of polarization-dependent interfacial structural relaxation at PZT/STO interfaces by quantitative ABF imaging in the aberration-corrected STEM and demonstrate that the internal structure relaxation is the primary mechanism of polarization bound charge compensation for this system. In a domain with upward polarization, the width of the structural relaxation zone at the interface is ∼3.5 unit cells, while the structure changes are slight and exhibit a longer screening range (∼5.5 unit cells) in a domain with downward polarization. The presence of interfacial oxygen vacancies in a domain with upward polarization accounts for a narrower interfacial structural relaxation layer, which is supported by the phase-field simulation and EELS measurement. The finding of a polarization orientation-dependent interfacial structure provides valuable insights into understanding the asymmetric domain nucleation barriers, domain shape, and hysteresis loop during ferroelectric domain switching and domain retention behavior in ferroelectric devices.

P.G. acknowledges support from National Basic Research Program of China (2016YFA0300804, 2016YFA0300903), National Equipment Program of China (ZDYZ2015-1), the National Natural Science Foundation of China (51672007, 51502007, 51502032), National Equipment Program of China (ZDYZ2015-1), and the "2011 Program" Peking-Tsinghua-IOP Collaborative Innovation Centre for Quantum Matter and the National Program for Thousand Young Talents of China. X.X.C. and L.-Q.C. are supported by the US Department of Energy, Office of Basic Energy Sciences, Division of Materials Sciences and Engineering under Award No. DE-FG02-07ER46417. H.-J.L., Y.-L.H., and Y.-H.C. were supported by the Ministry of Science and Technology, ROC (MOST 103-2119-M-009-003-MY3), and Centre for Interdisciplinary Science of National Chiao Tung University. A part of this work was conducted at the Research Hub for Advanced Nano Characterization, The University of Tokyo, supported by "Nanotechnology Platform" (Project No. 12024046), sponsored by MEXT, Japan.

[1] T. Mitsui and J. Furuichi, Phys. Rev. **90**, 193 (1953).
[2] J. Junquera and P. Ghosez, Nature (London) **422**, 506 (2003).
[3] A. K. Tagantsev, L. E. Cross, and J. Fousek, *Domains in Ferroic Crystals and Thin Films* (Springer, Berlin, 2010).
[4] M. Stengel and N. A. Spaldin, Nature (London) **443**, 679 (2006).
[5] S. Hong, S. M. Nakhmanson, and D. D. Fong, Rep. Prog. Phys. **79**, 076501 (2016).
[6] R. Nelmes and W. Kuhs, Solid State Commun. **54**, 721 (1985).
[7] T. Shaw, S. Trolier-McKinstry, and P. McIntyre, Annu. Rev. Mater. Sci. **30**, 263 (2000).
[8] R. V. Wang, D. D. Fong, F. Jiang, M. J. Highland, P. H. Fuoss, C. Thompson, A. M. Kolpak, J. A. Eastman, S. K. Streiffer, A. M. Rappe, and G. B. Stephenson, Phys. Rev. Lett. **102**, 047601 (2009).
[9] X. Liu, Y. Wang, P. V. Lukashev, J. D. Burton, and E. Y. Tsymbal, Phys. Rev. B **85**, 125407 (2012).
[10] H. Lu, C. W. Bark, D. Esque de los Ojos, J. Alcala, C. B. Eom, G. Catalan, and A. Gruverman, Science **336**, 59 (2012).
[11] D. D. Fong, G. B. Stephenson, S. K. Streiffer, J. A. Eastman, O. Auciello, P. H. Fuoss, and C. Thompson, Science **304**, 1650 (2004).
[12] S. Liu, I. Grinberg, and A. M. Rappe, Nature (London) **534**, 360 (2016).
[13] P. Gao, J. Britson, J. R. Jokisaari, C. T. Nelson, S.-H. Baek, Y. Wang, C.-B. Eom, L.-Q. Chen, and X. Q. Pan, Nat. Commun. **4**, 2791 (2013).
[14] D. D. Fong, A. M. Kolpak, J. A. Eastman, S. K. Streiffer, P. H. Fuoss, G. B. Stephenson, C. Thompson, D. M. Kim, K. J. Choi, C. B. Eom, I. Grinberg, and A. M. Rappe, Phys. Rev. Lett. **96**, 127601 (2006).
[15] N. Nakagawa, H. Y. Hwang, and D. A. Muller, Nat. Mater. **5**, 204 (2006).
[16] C. T. Nelson, P. Gao, J. R. Jokisaari, C. Heikes, C. Adamo, A. Melville, S.-H. Baek, C. M. Folkman, B. Winchester, and Y. Gu, Science **334**, 968 (2011).
[17] P. Gao, C. T. Nelson, J. R. Jokisaari, S.-H. Baek, C. W. Bark, Y. Zhang, E. Wang, D. G. Schlom, C.-B. Eom, and X. Pan, Nat. Commun. **2**, 591 (2011).

[18] C.-G. Duan, R. F. Sabirianov, W.-N. Mei, S. S. Jaswal, and E. Y. Tsymbal, Nano Lett. **6**, 483 (2006).
[19] P. Gao, C. T. Nelson, J. R. Jokisaari, Y. Zhang, S. H. Baek, C. W. Bark, E. Wang, Y. Liu, J. Li, C. B. Eom, and X. Pan, Adv. Mater. **24**, 1106 (2012).
[20] D. D. Fong, C. Cionca, Y. Yacoby, G. B. Stephenson, J. A. Eastman, P. H. Fuoss, S. K. Streiffer, C. Thompson, R. Clarke, R. Pindak, and E. A. Stern, Phys. Rev. B **71**, 144112 (2005).
[21] V. Nagarajan, J. Junquera, J. Q. He, C. L. Jia, R. Waser, K. Lee, Y. K. Kim, S. Baik, T. Zhao, R. Ramesh, P. Ghosez, and K. M. Rabe, J. Appl. Phys. **100**, 051609 (2006).
[22] S. Sadewasser, P. Jelinek, C. K. Fang, O. Custance, Y. Yamada, Y. Sugimoto, M. Abe, and S. Morita, Phys. Rev. Lett. **103**, 266103 (2009).
[23] P. Gao, H. J. Liu, Y. L. Huang, Y. H. Chu, R. Ishikawa, B. Feng, Y. Jiang, N. Shibata, E. G. Wang, and Y. Ikuhara, Nat. Commun. **7**, 11318 (2016).
[24] P. Gao, J. Britson, C. T. Nelson, J. R. Jokisaari, C. Duan, M. Trassin, S.-H. Baek, H. Guo, L. Z. Li, Y. Wang, Y.-H. Chu, A. M. Minor, C.-B. Eom, R. Ramesh, L.-Q. Chen, and X. Q. Pan, Nat. Commun. **5**, 3801 (2014).
[25] C. L. Jia, S. B. Mi, K. Urban, I. Vrejoiu, M. Alexe, and D. Hesse, Nat. Mater. **7**, 57 (2008).
[26] Y. Tang, Y. Zhu, X. Ma, A. Y. Borisevich, A. N. Morozovska, E. A. Eliseev, W. Wang, Y. Wang, Y. Xu, and Z. Zhang, Science **348**, 547 (2015).
[27] Y. L. Tang, Y. L. Zhu, Y. Liu, Y. J. Wang, and X. L. Ma, Nat. Commun. **8**, 15994 (2017).
[28] A. K. Yadav, C. T. Nelson, S. L. Hsu, Z. Hong, J. D. Clarkson, C. M. Schleputz, A. R. Damodaran, P. Shafer, E. Arenholz, L. R. Dedon, D. Chen, A. Vishwanath, A. M. Minor, L. Q. Chen, J. F. Scott, L. W. Martin, and R. Ramesh, Nature (London) **530**, 198 (2016).
[29] M. F. Chisholm, W. Luo, M. P. Oxley, S. T. Pantelides, and H. N. Lee, Phys. Rev. Lett. **105**, 197602 (2010).
[30] A. Y. Borisevich, H. J. Chang, M. Huijben, M. P. Oxley, S. Okamoto, M. K. Niranjan, J. D. Burton, E. Y. Tsymbal, Y. H. Chu, P. Yu, R. Ramesh, S. V. Kalinin, and S. J. Pennycook, Phys. Rev. Lett. **105**, 087204 (2010).
[31] Y. M. Kim, J. He, M. D. Biegalski, H. Ambaye, V. Lauter, H. M. Christen, S. T. Pantelides, S. J. Pennycook, S. V. Kalinin, and A. Y. Borisevich, Nat. Mater. **11**, 888 (2012).
[32] H. J. Chang, S. V. Kalinin, A. N. Morozovska, M. Huijben, Y. H. Chu, P. Yu, R. Ramesh, E. A. Eliseev, G. S. Svechnikov, S. J. Pennycook, and A. Y. Borisevich, Adv. Mater. **23**, 2474 (2011).
[33] P. Gao, A. Kumamoto, R. Ishikawa, N. Lugg, N. Shibata, and Y. Ikuhara, Microsc. Microanal. **22**, 888 (2016).
[34] C. L. Jia, K. W. Urban, M. Alexe, D. Hesse, and I. Vrejoiu, Science **331**, 1420 (2011).
[35] S.-B. Mi, C.-L. Jia, I. Vrejoiu, M. Alexe, and D. Hesse, Adv. Mater. Interfaces **2**, 1500087 (2015).
[36] L. W. Chang, M. Alexe, J. F. Scott, and J. M. Gregg, Adv. Mater. **21**, 4911 (2009).
[37] See Supplemental Material at http://link.aps.org/supplemental/10.1103/PhysRevB.97.180103 for additional experimental and calculation details.
[38] W. Zhong, R. D. King-Smith, and D. Vanderbilt, Phys. Rev. Lett. **72**, 3618 (1994).
[39] R. E. Cohen, Nature (London) **358**, 136 (1992).
[40] C. Lichtensteiger, J. M. Triscone, J. Junquera, and P. Ghosez, Phys. Rev. Lett. **94**, 047603 (2005).
[41] G. Gerra, A. K. Tagantsev, N. Setter, and K. Parlinski, Phys. Rev. Lett. **96**, 107603 (2006).
[42] Y. Li, S. Hu, Z. Liu, and L. Chen, Acta Mater. **50**, 395 (2002).
[43] Y. L. Li, S. Y. Hu, Z. K. Liu, and L. Q. Chen, Appl. Phys. Lett. **81**, 427 (2002).
[44] Q. Qiao, Y. Zhang, R. Contreras-Guerrero, R. Droopad, S. T. Pantelides, S. J. Pennycook, S. Ogut, and R. F. Klie, Appl. Phys. Lett. **107**, 201604 (2015).
[45] H. W. Jang, D. A. Felker, C. W. Bark, Y. Wang, M. K. Niranjan, C. T. Nelson, Y. Zhang, D. Su, C. M. Folkman, S. H. Baek, S. Lee, K. Janicka, Y. Zhu, X. Q. Pan, D. D. Fong, E. Y. Tsymbal, M. S. Rzchowski, and C. B. Eom, Science **331**, 886 (2011).
[46] D. A. Muller, N. Nakagawa, A. Ohtomo, J. L. Grazul, and H. Y. Hwang, Nature (London) **430**, 657 (2004).
[47] A. N. Morozovska, E. A. Eliseev, A. K. Tagantsev, S. L. Bravina, L.-Q. Chen, and S. V. Kalinin, Phys. Rev. B **83**, 195313 (2011).
[48] Y. M. Kim, A. Morozovska, E. Eliseev, M. P. Oxley, R. Mishra, S. M. Selbach, T. Grande, S. T. Pantelides, S. V. Kalinin, and A. Y. Borisevich, Nat. Mater. **13**, 1019 (2014).
[49] V. Nagarajan, S. Prasertchoung, T. Zhao, H. Zheng, J. Ouyang, R. Ramesh, W. Tian, X. Q. Pan, D. M. Kim, C. B. Eom, H. Kohlstedt, and R. Waser, Appl. Phys. Lett. **84**, 5225 (2004).
[50] H. Lu, X. Liu, J. D. Burton, C. W. Bark, Y. Wang, Y. Zhang, D. J. Kim, A. Stamm, P. Lukashev, D. A. Felker, C. M. Folkman, P. Gao, M. S. Rzchowski, X. Q. Pan, C. B. Eom, E. Y. Tsymbal, and A. Gruverman, Adv. Mater. **24**, 1209 (2012).